Phase Image Texture Analysis for Motion Detection in Diffusion MRI (PITA-MDD)

Nahla M H Elsaid PhD[1] | Jerry L Prince PhD[2] | Steven Roys MSc[3] | Rao P Gullapalli PhD[3] | Jiachen Zhuo PhD[3]

[1]Department of Radiology and Imaging Sciences, Indiana University School of Medicine, Indianapolis, IN, United States.
[2]Electrical and Computer Engineering, Johns Hopkins University, MD, United States.
[3]Diagnostic Radiology, University of Maryland School of Medicine, Baltimore, MD, United States.

Correspondence to:
Nahla M H Elsaid PhD, 355 West 16th Street, Suite 4100, Indianapolis, IN, 46202 Email: nelsaid@iu.edu

Abstract

Purpose:

Pronounced spin phase artifacts appear in diffusion-weighted imaging (DWI) with only minor subject motion. While DWI data corruption is often identified as signal drop out in diffusion-weighted (DW) magnitude images, DW phase images may have higher sensitivity for detecting subtle subject motion.

Methods:

This article describes a novel method to return a metric of subject motion, computed using an image texture analysis of the DW phase image. This Phase Image Texture Analysis for Motion Detection in dMRI (PITA-MDD) method is computationally fast and reliably detects subject motion from diffusion-weighted images. A threshold of the motion metric was identified to remove motion-corrupted slices, and the effect of removing corrupted slices was assessed on the reconstructed FA maps and fiber tracts.

Results:

Using a motion-metric threshold to remove the motion-corrupted slices results in superior fiber tracts and fractional anisotropy maps. When further compared to a state-of-the-art magnitude-based motion correction method, PITA-MDD was able to detect comparable corrupted slices in a more computationally efficient manner.

Conclusion:

In this study, we evaluated the use of DW phase images to detect motion corruption. The proposed method can be a robust and fast alternative for automatic motion detection in the brain with multiple applications to inform prospective motion correction or as real-time feedback for data quality control during scanning, as well as after data is already acquired.

2

INTRODUCTION

Diffusion magnetic resonance imaging (d-MRI) has been proven to be a useful tool to identify microstructure changes, particularly in the brain. As diffusion imaging measures the microscopic movement of water molecules, it is extremely sensitive to the subject's macroscopic or bulk motion. Any bulk motion during the diffusion encoding of the sequence can cause severe signal loss, leading to erroneous diffusion tensor reconstruction. Three main categories of bulk motion affect diffusion imaging: the motion due to respiratory and cardiac cycles, the vibrational motion of patient table due to the application of diffusion gradients, and the subject's bulk head-motion, all of which could cause substantial image artifacts. Cardiac gating can be used to avoid corruption due to cardiac pulsation [1] [2]. The vibrational motion can be mitigated by using phase encoding (PE) reversal and then combining the blip-up and blip-down images as in the COVIPER method [3] or through improved hardware design of the MRI scanner. While single shot diffusion-weighted EPI could reduce the effect of bulk subject motion as it is less sensitive to phase errors, it cannot overcome severe bulk motion as in the case of the involuntary motion of patients with Parkinson's disease [4] or motion in young children [5]. Head motion in those cases can lead to inaccurate tensor estimation, which in return leads to erroneous fiber tracking and maps pertaining to different diffusion metrics. In some cases, the scans must be repeated with the hopes that no motion occurs in the repeated scan. In other severe cases of motion, a given study might be discarded or used with compromised reliability, which may have implications in analysis outcome.

Diffusion tensor imaging (DTI) could be improved by incorporating a quality measure of each diffusion-weighted image and removing motion-corrupted data before data analysis. Computing such quality measures based on the magnitude images followed by data rejection of the diffusion-weighted images has been proposed previously. Two of these methods, dubbed RESTORE and iRESTORE, were based on the voxel-wise identification of outliers in nonlinear diffusion tensor estimators [6] [7]. A slice based identification method called *eddy* [8] [9] (included in the FSL software package (FMRIB, Oxford, UK)) detects slices affected by magnitude signal loss through a nonparametric prediction using an iterative Gaussian process. Another method based on local binary patterns to extract texture features from the DWI data was presented in [10]. In [11], a k-space based method was briefly described, where higher entropy of the k-space was correlated with slice motion. A volume-based quality control method in the form of open source DTIPrep software was proposed in [12] [13]. While all of these methods are effective, their computational demands are high and therefore are not suitable for real-time applications.

Rigid body motion during diffusion-weighted imaging affects the MR signal by a phase error, primarily when the motion occurs during the diffusion gradient encoding step [14] [15] [16]. This type of motion usually results in signal dropouts that can be mitigated primarily by discarding the corrupted slices [17] [18] [19]. For instance, Fig. 1a shows examples of DWI magnitude images and Fig. 1b shows their corresponding phase images; it can be observed that phase images appear to distinguish slices with motion more efficiently. Although previous methods have focused on the impact of motion on the

3

magnitude images, we suggest that the direct examination of the phase images themselves could lead to a reliable measure for data corruption.

In this paper, we present a novel phase-based metric to detect motion in diffusion-weighted images. This Phase Image Texture Analysis for Motion Detection in dMRI (PITA-MDD) method is computationally fast and can reliably detect subject motion.

The PITA-MDD method is based on the observation that Haralick's textural features [20] applied to phase images are more sensitive in detecting subject motion than an existing state-of-the-art method (*eddy*) [8] when applied to the corresponding diffusion-weighted magnitude images. The PITA-MDD method was briefly described in [21], where one experiment was presented showing a comparison between the detected motion using the current method versus that detected using an external motion tracking sensor, indicating a good agreement. In this paper, we examined the method's performance on diffusion tensor imaging of the brain and compared the results to the technique included in the eddy package [8]. Moreover, we validated the PITA-MDD method by analyzing the motion detection threshold using seven datasets where two dMRI repetitions were acquired, one with motion and another without motion. We used the FA map of the motion free repetition of each subject as the gold standard and compared the FA map reconstructed using different motion detection/rejection thresholds based on the Normalized Absolute Error (NAE) of the FA maps.

This study has two main objectives. The first objective is to propose a new phase-based algorithm that can detect subject motion from diffusion-weighted images. The second objective is to validate the method using: (a) across-subject stability test, (b) across imaging protocol stability test, (c) comparison to a state-of-the-art magnitude-based motion correction method, and (d) noise simulation. Results indicate that the proposed method is reasonably accurate and computationally fast, and will, therefore, lend itself to real-time detection of motion in DWI data.

MATERIAL AND METHODS

Fig. 2 provides a block diagram of the PITA-MDD method, which we briefly overview here and then describe in detail below. The method starts with the acquisition of DWI data (including both magnitude and phase images). A volume-of-interest-mask of the brain is automatically extracted from the b_0 volume, and the phase images are multiplied by the calculated mask. A gray level co-occurrence matrix (one of Haralick's textural features) is then computed for each phase image, and then Haralick's homogeneity index is computed from this as a quality metric for each diffusion-weighted image. Haralick's homogeneity index was chosen as it reflects the degree of homogeneity in the phase image.

A threshold T (the determination of which is described in section 2.3) is used to identify the motion-corrupted slices (i.e., a slice acquired with a diffusion weighting gradient) which are purged before DTI reconstruction. The validation of our method is based on comparing FA maps calculated using a cleaned dataset that was contaminated with motion, against those from a dataset without deliberate

4

motion. In addition, our method was compared with the well-established *eddy* tool for its sensitivity to motion-corruption detection in DWI data.

2.1 Theory

Both microscopic and bulk motion are encoded as phase variations in the presence of diffusion encoding gradients. Microscopic motion (on the order of tens or hundreds of microns), i.e., the diffusion motion that we want to encode, only manifests as a small phase variation across the brain [15]. While microscopic motion could induce phase in the image, it would need to be coherent motion. However, microscopic diffusion motion induces incoherent phase in the signal, which leads to signal attenuation. Accordingly, the resulting phase image appears smooth or homogeneous, which is captured as a high homogeneity value using the Haralick's homogeneity index (HHI). The b_0 volume, lacking any diffusion encoding, represents the most homogeneous phase image, which in turn has the highest homogeneity value. In the case of bulk motion (on the order of mm), even small head rotations lead to larger phase variations in the presence of diffusion encoding gradients. By considering the phase wrapping effect, a significant phase variation can lead to high-frequency ripples in the DW phase images resulting in a low homogeneity value as captured by the HHI. Magnitude signal dropout will occur when large phase variations have been produced, which is also termed as spin de-phasing. This explains why our PITA-MDD method is more sensitive than the magnitude-based methods in detecting subject motion.

In the following analysis, we assume that subject motion during the diffusion sensitizing gradients will have a more prominent effect on image phase than motion occurring during the imaging gradients. Consider a particular spin with a time-varying gradient $\vec{G}$ and a position $\vec{r}$ in the gradient coordinate system. Adopting the convention presented in [22] for infinitesimal rotation (rotation with a very small angle, in which the sum of infinitesimal rotations does not depend on the order of the rotations), a bulk motion in the form of rotation with a rotation vector $\vec{\Omega}$ and a translation from the position $\vec{r}$ through the displacement vector $\vec{S}$ causes a phase shift $\Delta\varphi$ as detailed in [14]:

$$\Delta\varphi(\vec{r}, t) = \gamma \int_0^t d\tau [\vec{\Omega} \times \vec{G}(\tau)] . \vec{r} + \gamma \int_0^t \vec{G}(\tau)\vec{S}(t)d\tau, \tag{1}$$

where γ is the gyromagnetic ratio, t represents a general time variable, and τ is a dummy variable of integration. The first term of the right-hand side of Eq. (1) is due to rotation, which causes a linear phase ramp producing blurring or signal dropout in the resulting magnitude images. The second term, which is due to translation, causes only a global phase shift in the resulting phase image.

In DW brain imaging, head rotations are common, and the resulting motion can cause severe phase variations within the images. If the phase ramp in Eq.(1) approaches or exceeds π radian/voxel, then the phase dispersion within a single voxel will be large enough to cause significant signal attenuation [23]. This dropout is what magnitude-based motion detection algorithms rely on to detect motion in DW acquisitions. For smaller motions, where the magnitude image may not experience much signal

5

attenuation, the phase variations across the image will still be evident as multiple phase edges (caused by phase wrapping). These phase edges alter the textural homogeneity of the phase image, which is usually quite apparent to the naked eye. If this textural inhomogeneity can be automatically detected, it may prove to be more sensitive than magnitude-based detection and may eventually lead to a more practical real-time detection solution.

The gray level co-occurrence matrix (GLCM) of an image, which we denote by p, is defined as the distribution (normalized histogram) of co-occurring values at a given spatial offset [20]. The GLCM was computed by first dividing the image into g gray levels, where g is an integer, which means that the GLCM will be a g by g matrix. Four GLCMs were computed using pixel offsets in the four different directions of adjacencies (horizontal, vertical, and left and right diagonals) and were averaged to obtain a final co-occurrence matrix. Three examples of GLCMs are shown in Fig. 3, for phase images with no motion, subtle motion, and severe motion. In this example, phase values were quantized to just eight discrete levels between $-\pi$ and π and the offset was one pixel in the horizontal direction. We then extract Haralick's homogeneity index (HHI) for each DWI slice from the resulting GLCM as follows,

$$HHI = \sum_{i,j} \frac{p(i,j)}{1+|i-j|}$$ (2)

where $p(i,j)$ denotes element (i,j) in the GLCM matrix.

The HHI is a good indicator of the extent of motion present in the corresponding DWI. If the phase image is corrupted with motion, HHI has a low value, as shown in Fig. 3h. In contrast, high values of HHI are indicative of no motion. Our method for defining a threshold on HHI to identify motion-corrupted images is described below.

2.2 Data Acquisition

We acquired diffusion-weighted images (both magnitude and phase) on two scanners, a 3T Prisma[fit] and a 3T Tim Trio (Siemens Healthcare, Erlangen, Germany). In the case of the Tim Trio scanner, we used a 12-channel head coil, and in the case of the Prisma[fit] scanner, we used a 64-channel head and neck coil. Seven datasets were acquired on five healthy volunteers. We refer to the volunteers as V1, V2, V3, V4, and V5. The volunteers were instructed to rotate their heads voluntarily by an angle (around 1 to 5 degrees) for about 5 seconds, and then to return their heads to the original position after movement. They were also given a button box during imaging and instructed to press buttons whenever they moved their head. The study was approved by the Institutional Review Board at the University of Maryland School of Medicine, and all participants provided written informed consent.

The dMRI protocols are as follows:

Protocol 1 (Prisma[fit]): Single Shot 2D spin-echo echo planar imaging (EPI) was applied with TR 5.4 s, TE 66 ms, field of view 240 mm, 54 slices, 2.5 mm slice thickness, matrix size 96 x 96 (image pixel size 2.5 mm x 2.5 mm), bandwidth 2480 Hz/Px, full k-space, GRAPPA iPAT mode with PE acceleration factor of 2, and 0.49 ms echo spacing. Diffusion parameters: b-value= 1000 s/mm^2, bipolar diffusion scheme, 5

6

non-diffusion weighted volumes and 63 diffusion gradient directions, 2 repetitions except for V5 on whom only a single repetition data was obtained. Slices were interleaved, and images were reconstructed as both magnitude and phase images on the scanner.

Protocol 2 (Prisma[fit]): Single Shot 2D spin-echo echo planar imaging (EPI) with: TR 5.9 s TE 72 ms, field of view 240 mm, 54 slices, 2 mm slice thickness, matrix size 118 x 118 (image pixel size 2 mm x 2 mm), bandwidth 2230 Hz/Px, full k-space, GRAPPA iPAT mode with PE acceleration factor of 2, and 0.53 ms echo spacing. Diffusion parameters: b-value= 1000 s/mm^2, bipolar diffusion scheme, 5 non-diffusion weighted volumes 63 diffusion gradient directions, 2 repetitions.

Protocol 3 (Tim-Trio): Single Shot 2D spin-echo echo planar imaging (EPI) was applied with TR 5 s, TE 79 ms, field of view 240 mm, 45 slices, 3 mm slice thickness, matrix size 80 x 80 (image pixel size 3 mm x 3 mm), bandwidth 2604 Hz/Px, full k-space, no PAT, and 0.47 ms echo spacing. Diffusion parameters: b-value=1000 s/mm^2, bipolar diffusion scheme, 4 non-diffusion weighted volumes, 30 electrostatically arranged diffusion gradient directions [24], two repetitions. Images were obtained from all five volunteers using Protocol 1, and this dataset was used to test the stability of the proposed method across subjects. Volunteer V1 was scanned using both Protocol 1 and 2 and was also scanned using Protocol 3 on a separate day (8 months apart), to assess the robustness of the results from multiple scans on the same subject.

2.3 Data Processing

Cleaning Slices with Motion

All procedures were developed in Matlab (The MathWorks, Inc., Natick, MA). We used motion estimation [25] [26] with the magnitude images to confirm that the motion during the no motion case was not more than 1.3 mm. The phase images were first multiplied by a brain mask generated using the FSL tool (BET) [27] applied on the b_0 images; the mask was regularly updated by the new b_0 images. Before computing the GLCM of the phase images, the area outside of the brain was excluded.

Haralick's Homogeneity index (HHI) was then computed using Eq. (2), yielding an HHI for each slice per gradient direction in each dataset. We used a cut-off threshold T, the determination of which will be explained in the next subsection. Those images with $HHI < T$ were excluded from tensor reconstruction (and all subsequent standard downstream computations). The elapsed CPU time for running the algorithm on one slice is 2.15 ms on average.

Determination of the Cut-off threshold

In all our experiments with two repetitions (V1 to V4), volunteers were instructed to move only in the second repetition, Thus, in those experiments, we consider the diffusion tensor reconstructed from the first repetition as the ground truth to determine our motion detection threshold (cutoff threshold). During further data inspection, data from volunteer V4 appeared to contain small motion artifact in the first repetition, therefore five total datasets was used in this step of processing. DTI reconstruction was performed on both the clean data (first repetition) and motion corrupted data (second repetition). DTI

7

reconstruction was performed on both the clean data (first repetition) and motion corrupted data (second repetition). Motion rejection with cutoff thresholds ranging from 0 to 0.9 was applied on the motion corrupted data, and the resulting FA maps were compared to the FA map from the clean data based on the NAE. The optimal threshold that results in the least error from the ground truth FA map was calculated for each dataset to assess the sensitivity of FA computations to the cutoff threshold. Then a cutoff-threshold was determined using the minimum of the sum of squares of the FA errors for all compared datasets.

DTI reconstruction

Diffusion-weighted images before and after removing motion corrupted slices were processed using the Diffusion Toolkit script [28] to estimate the diffusion tensors and the corresponding DTI feature maps. Fiber tracts were visualized using TrackVis software [28]. The TrackVis program uses an interpolated streamline approach to reconstruct fiber paths. We used an angle threshold of 27° to compare the fiber tracts with and without motion removal.

2.4 Validation

Comparison to eddy method

Eddy is a well-established software tool [9] which uses a statistical method to detect the outlier slices based on comparing the expected signal in a DW magnitude image using the neighboring slices in the Q-space to the signal observed in the actual slice. This tool is available as a part of the FSL package version 5.0.10 (FMRIB, Oxford, UK). The identified motion corrupted slices from *eddy* were compared against our results.

Noise Simulation

To simulate the effect of phase noise in identifying motion corrupted slices, Gaussian random noise with zero mean was added simultaneously to the real and imaginary part of the images (calculated using the phase and magnitude images). Six levels of noise with standard deviations (SD) = 5, 15, 25, 35, 45, and 55 were added to the whole dataset of V1 at three different resolutions of 3 mm isotropic, 2.5 mm isotropic and 2 mm isotropic. We ran both PITA-MDD and *eddy* on the three resolutions, each at the six levels of noise to test the sensitivity of both methods to noise. To examine the sensitivity of the HHI to noise, Gaussian random noise with zero mean and SD that varies between 0 and 60 were added to three slices (in three different resolutions) with HHI in the range between 0.65 and 0.685 and another set of three slices with HHI in the range between 0.92 and 0.98. We further measure the SNR (with different level of added noise) by computing the ratio of the mean of the intensity of the voxels inside an arbitrary region inside the brain to the standard deviation of the intensity of voxels inside a region in the background.

8

RESULTS

3.1. Motion Detection with HHI

The left column of Fig. 4a shows the homogeneity textural feature, HHI, extracted from the DW phase images of the five volunteers per slice over the entire dMRI acquisition using imaging Protocol 1. It is observed that the locations and number of HHI drops in each scan match the time and the number of times the volunteers pressed a button to indicate that they are moving at the time during the d-MRI scans. It should be noted that HHI is substantially higher during the b_0 volumes than in the volumes with applied diffusion gradient as the phase images in the former case are more homogeneous. The right column of Fig. 4a shows the histogram distribution of HHI for the entire DWI acquisition for each subject. In the same column, the small peaks to the left of the main peaks in the histogram plots indicate Haralick's homogeneity indices corresponding to motion corrupted slices. The chosen T threshold (T = 0.56, please see details in section 3.2) reliably marked HHI's and the corresponding DWI slices to be removed before diffusion tensor estimation. Fig. 4b shows a set of cases with different motion patterns and the resulting HHI distribution of V1. Fig. 4b (rows 1-3) show the histogram distributions of HHI for the entire DWI acquisition for the same subject with different resolutions (3 mm x 3 mm), (2.5 mm x 2.5 mm) and (2 mm x 2 mm) respectively, and with different motion patterns. Fig 4b (row 4) shows HHI and the corresponding histogram distribution of V1 (2 mm x 2mm) without motion; note that the threshold (0.56) in this case will not reject any slices.

3.2. Determination and Validation of the Cut-off Threshold

As previously stated, in all our experiments the volunteers were instructed to move only during the second repetition of the dMRI acquisition, while the first repetition was free of motion and the corresponding reconstructed FA served as the ground truth.

Fig. 5 shows the motion rejection threshold versus the normalized absolute error (NAE) between the FA maps of the motion rejected data and that of the ground truth in each experiment. Five datasets V1 (3 mm x 3 mm), V1 (2.5 mm x 2.5 mm), V1 (2 mm x 2 mm), V2 and V3 were incorporated in this comparison. Fig. 5f shows the mean square of all the errors in the five cases by which we determine the threshold T with the minimum FA error to be equal to 0.56. It is an ideal value to use as it is also roughly in the center of the low plateau of the FA error. We, therefore, use T=0.56 for the following motion rejection analysis.

3.3 Across Subject Stability

Table 1 shows the percentage of the detected corrupted slices using the PITA-MDD method and the T threshold. Using Protocol 1, rejected motion corrupted data using PITA-MDD ranges from 0.83% to 2.84%. Please see section 3.5 for the comparison of the PITA-MDD results with that of *eddy*.

Fig. 6 shows axial and coronal FA maps calculated with all the acquired images versus the maps calculated with the detected motion-corrupted slices removed. The quality of the FA maps calculated after eliminating the motion-corrupted slices is visually superior to the quality of the FA maps calculated using the complete dataset. For example, there are multiple axial slices that appear to be different from the surrounding tissues in the non-corrected images. This effect is indicated by horizontal edges in the coronal FA maps that should not be present.

Fig. 7a shows tractography results from a seed of a 1.25 voxel area in the Genu region that are compared before and after eliminating the slices corrupted with motion. Trackvis-filters (e.g. trajectories length threshold) were made consistent in both cases. Erroneous fiber tracts appear in the uncorrected data and are absent in the cleaned data.

3.4 Across Imaging Protocol Stability

Table 2 shows the percentage of the detected corrupted slices using our phase-based method on V1 using all three imaging protocols at different resolution scales. The phase-based method reliably detected all subjects' head motions as confirmed by button-pressing (as shown in Fig. 4.b). Fig. 7b shows the tractography using the whole datasets versus the tractography with the corrupted slices removed. Within all three resolutions, the quality of the fiber tracts after eliminating the corrupted slices clearly exceeds the quality of the fiber tracts generated by including the corrupted slices.

3.5. Comparison to *eddy*

We compared the detected motion corrupted slices using our phase-based method against those computed by *eddy* (Tables 1 and 2). Table 2 shows the percentage of detected corrupted slices using the PITA-MDD method versus the percentage of outliers using the *eddy* software in Protocol 2 for V1 using data obtained at different resolution scales.

In addition, Tables 1 and 2 show the detection overlap between the proposed method and [8]. The PITA-MDD method detected most of the motion corrupted slices that *eddy* detected. The PITA-MDD was more sensitive in picking up motion corruption compared to what may be evident in magnitude-based approaches (Fig. 8a). For more subtle motion where image blurring rather than apparent signal dropout was visible in magnitude images (slice 5 in Fig. 8a), the PITA-MDD method was able to identify corrupted-slices based on phase-image textural content. For large motions which are manifested by signal dropouts, both methods reliably detected them (slice 1 and 3).

Fig. 8b shows an example of some outlier slices that were identified by *eddy* but not by PITA-MDD. These slices represent examples of the issue outlined in [9] which pointed out that *eddy* can potentially discard valid data which could ideally be used as part of a slice-to-volume resampling scheme. It is also possible that PITA-MDD would miss slices where motion occurred outside the sensitizing gradients time window, while such displacement may be detected by *eddy*.

3.6. Noise Simulation

10

Fig. 9 shows an example of the magnitude and phase images of a DWI at three levels of Gaussian random noise. Assuming the data with no noise added to be the ground truth, Table 3 demonstrates the ability of the proposed method to detect motion corrupted slices with added noise. With increased noise, there is a slight increase in the percentage of slices detected by PITA-MDD and a slight decrease of the percentage of slices detected by *eddy*, while the common slices detected by both methods were consistent across noise levels. Figure 10 shows the sensitivity of the HHI in six different slices to added Gaussian random noise with zero mean and SD that ranges from 0 to 60, in a low HHI (Figure 10a) and high HHI (Figure 10b) scenarios. Both scenarios were illustrated by three different resolutions 3mm x 3mm, 2.5mm x 2.5 mm and 2mm x 2mm. In addition, the same figure shows the SNR values of the corresponding DWI slice with no added noise and with added Gaussian random noise with SD of 60. In both the low and high HHI scenarios, HHI showed a slight drop with the increased noise SD level, which is more visually apparent in the low HHI scenario. Such an HHI drop was also more apparent in the case of 3 mm resolution in the high HHI senario, as the DW image SNR was low (SNR < 2) even before adding the additional noise. The 3mm data set was acquired on an older scanner (Tim Trio), which resulted in the inherently lower SNR in the DWI. Nevertheless, the HHI reduction is less than 10% in all cases, and is less than 5% for added Gaussian random noise with SD of 40 or lower (DW image SNR of 1 or higher).

DISCUSSION

Motion-induced artifacts in MR diffusion imaging can produce noticeable artifacts in computed results such as FA and tractography. As demonstrated by [9], a rotational motion as small as $5°$ can cause a significant signal dropout that can reduce image quality. In this study, we have presented a novel method for detecting motion-corrupted slices. In addition, evidence has been provided that removing these slices from the diffusion tensor calculations leads to improvements in the quality of the diffusion maps and tractography. The PITA-MDD method is computationally fast and can reliably detect subject motion from diffusion-weighted images.

The amount of accumulated phase due to subject motion is affected by both the direction of motion and the direction of diffusion encoding gradient. Ignoring the effect of other imaging gradients, the motion perpendicular to the diffusion gradients produces no phase error. In the case of the well-padded subject head within a head coil, most motion artifacts come from rotational motion. In the event of rotational motion, if one component of the rotational motion is rotating around an axis non-parallel to the diffusion gradient, it will cause detectable phase errors in the phase images corresponding to signal dropouts or blurring in the magnitude images. While signal dropouts are easily detectable in magnitude methods, signal blurring may only be detected by the phase method.

The PITA-MDD method worked robustly in all experiments, as even a subtle motion could be detected by the current method. It should be noted that while the overall signal level may be preserved in

11

the presence of subtle motion, such images may be blurred and are easily missed by magnitude methods. However, unlike *eddy*, which is a global method that can reject slices due to their displacements relative to the whole volume, the PITA-MDD method can detect motion in a slice regardless of its location relative to the whole volume. That PITA-MDD trait can address the issue noted by [9] of potentially rejecting valid data that can possibly be used as a part of slice-to-volume registration. Although magnitude information alone is usually used in slice-to-volume correction, our results suggest that phase information might also be used as independent guidance for this process. On the other side, when there is motion, merely discarding slices does not correct for head displacement. Accordingly, motion correction as a part of standard dMRI preprocessing should be used in conjunction with robust methods to correct for head displacement between volumes.

It is worth noting that the b-value used in all the experiments was 1000 s/mm^2, as it is the most common value used in many applications. While we did not test the technique at other b-values, we expect that the proposed PITA-MDD method will remain sensitive to motion compared to magnitude based methods of detection even at lower b-values as demonstrated in [29]. However, when using the method with a multi-shell regime it is advisable to use a threshold that changes according to the b-value of the slice instead of the fixed threshold value used here. There are different scenarios where different weighting schemes should be considered: 1) in cases of mildly corrupted (blurred) slices, where part of the gathered information could still be useful and 2) for non-rigid motion where blurring or dropouts may only affect certain areas of the image. The latter scenario is true for high b-value imaging where the pulsatile motion becomes more relevant and where spatially varying low SNR is a limitation for detection. Future studies are needed to investigate the ideal weighting regime in those cases. In addition, a limitation of the current method is that it uses a fixed threshold of T=0.56, based on the training data. A possible extension of the method would be to use statistical techniques to identify the threshold from the data itself.

It is expected that the method could easily be applicable to image other body parts where lower b-value is used, for example in cardiac d-MRI [30] or tongue d-MRI [31] [29]. As demonstrated by the noise simulation, the HHI can be affected by very low SNR in DW images (e.g. SNR < 1). Such HHI decrease leads to a maximum of 1.42% more slices being detected as motion corrupted slices in our noise simulation. Thus, we infer that PITA-MDD will still have high sensitivity to motion at higher b-values, with a minor tendency of producing false positive results. On the other hand, the method has a low sensitivity to detect motion in low b-value images, particularly for b_0 images. Accordingly, a possible extension of the developed method might be to fuse magnitude and phase correction methods for the detection of motion across the whole range of b-values. As seen in Figure 4, the HHI curves show periodic drops related to TR that are correlated to the edge brain slices which contain little brain tissues leading the HHI to drop. The performance of the HHI at the edge slices could potentially be improved using robust normalization across slices, for example, using normalization coefficients from training data.

12

A possible extension of this work is to examine the efficiency of the method with well-quantified types of motion (rotation and translation) as well as with different speeds to analyze the sensitivity of the method pertaining to motion direction and motion speed. This is readily available in other tools for diffusion processing [8], [32]. The significance of the presented method is its ability to detect slices with motion in real time (i.e., motion detection and feedback during the scanning for quick assessment of data quality immediately post-acquisition). The PITA-MDD method could be added to any scanner for online motion detection in d-MRI. This can have multiple applications either for prospective motion correction, as real-time feedback for data quality control. An example to use the method is to process each slice phase image to provide an indication to the scanner operator whether the data is expected to be reliable or not.

Notice that we used five non-diffusion weighted volumes per repetition and the generated brain mask was used to update HHI calculation. These are only needed if a severe motion is anticipated so that the mask used in HHI calculation would accurately reflect the actual brain position. From our experience, the HHI calculations are only slightly affected by a small inaccuracy of the brain mask for most brain slices, although edge slices where the brain encompasses a very small region within the slice can also be affected. Overall acquisitions with only one b_0 volume and a single brain mask are unlikely compromised, especially when the subject's head is well padded, and motion is mostly rotational.

This research proposes a robust method to detect motion in real time. One limitation of this method is that it requires phase maps, which may require additional steps to obtain from the scanner. We note, however, that manufacturers usually allow the reconstruction of DWI phase maps on the scanner without pulse sequence modification. Another limitation of this method is that it is only validated for diffusion-weighted images with b-value of 1000 s/mm^2. In the future, sensitivity analysis of this method similar to that presented in [33] could be employed to study the interdependence of the number of quantization levels and offsets used for GLCM computation against the SNR, resolution, and b-value (dynamic range) of the phase data. In addition, the method could be extended by using modern definitions of the Haralick's descriptors such as those presented in [34] which introduced Haralick features that are invariant to the number of quantization gray-levels.

CONCLUSIONS

In this study, we evaluated the use of DW phase images to detect motion corruption. The proposed method can be a robust and fast alternative for automatic motion detection. Our results demonstrate that the proposed phase-based method produces comparable results to those of the magnitude-based methods. The difference in the detected slices between the phase-based method and the magnitude methods could be attributed to the blurred images (as shown in Fig. 8a) where the phase-based method could detect these blurred slices. The PITA-MDD method has multiple applications for

13

either prospective motion correction or as real-time feedback for data quality monitoring during scanning, and after data is already acquired.

Acknowledgments

REFERENCES

[1] S. Skare and J. Andersson, "On the effects of gating in diffusion imaging of the brain using single shot EPI," *Magn Reson Imaging,* vol. 19, pp. 1125-1128, 2001.

[2] R. Nunes, P. Jezzard and S. Clare, "Investigations on the efficiency of cardiac-gated methods for the acquisition of diffusion weighted images," *J Magn Reson,* vol. 177, pp. 102-110, 2005.

[3] S. Mohammadi, Z. Nagy, C. Hutton, O. Josephs and N. Weiskopf, "Correction vibration artifacts in DTI using phase–encoding reversal COVIPER).," *Magn Res Med,* vol. 68, pp. 882-889, 2012.

[4] R. Perea, R. Rada, J. Wilson, E. Vidoni, J. Morris, K. Lyons, R. Pahwa, J. Burns and R. Honea, "A comparative white matter study with Parkinson's disease, Parkinson's disease with Dementia and Alzheimer's disease.," *J Alzheimers Dis Parkinsonism,* vol. 3, pp. 123-139, 2013.

[5] L. Walker, L. Chang, A. Nayak, M. Irfanoglu, K. Botteron, J. McCracken, R. McKinstry, M. Rivkin, D. Wang, J. Rumsey and C. Pierpaoli, "The diffusion tensor imaging (DTI) component of the NIH MRI study of normal brain development (PedsDTI)," *Neuroimage,* vol. 124 Part B, pp. 1125-1130, 2016.

[6] L. Chang, D. Jones and C. Pierpaoli, "RESTORE: robust estimation of tensors by outlier rejection," *Magn Res Med,* vol. 53, p. 1088–1095, 2005.

[7] L. Chang, L. Walker and C. Pierpaoli, "Informed RESTORE: A method for robust estimation of diffusion tensor from low redundancy datasets in the presence of physiological noise artifacts," *Magn Res Med,* vol. 68, pp. 1654-1663, 2012.

[8] J. Andersson and S. Sotiropoulos, "An integrated approach to correction for off-resonance effects and subject movement in diffusion MR imaging," *NeuroImage,* vol. 125, pp. 1063-1078, 2016.

[9] J. Andersson, M. Graham, E. Zsoldos and S. Sotiropoulos, "Incorporating outlier detection and replacement into a non-parametric framework for movement and distortion correction of diffusion MR images," *NeuroImage,* vol. 141, pp. 556-572, 2016.

[10] Z. Zhou, W. Liu, J. Cui, X. Wang, D. Arias, Y. Wen, R. Bansal, X. Hao, Z. Wang, B. Peterson and D. Xu, "Automated artifact detection and removal for improved tensor estimation in motion-corrupted DTI data sets using the combination of local binary patterns and 2D partial least squares," *Magn Reson Imaging,* vol. 29, pp. 230-242, 2011.

[11] S. Holdsworth, S. Skare and R. Bammer, "On the application of phase correction and use of k-space entropy in partial Fourier diffusion-weighted EPI," in *17th Annual Meeting ISMRM*, Honolulu, 2009.

[12] Z. Liu, Y. Wang, G. Gerig, S. Gouttard, R. Tao, T. Fletcher and M. Styner, "Quality Control of Diffusion

14

Weighted Images," *Proceedings of SPIE--the International Society for Optical Engineering,* 2010.

[13] I. Oguz, F. Mahshid, J. Matsui, F. Budin, Z. Liu, G. Gerig, H. Johnson and M. Styner, "DTIPrep: quality control of diffusion-weighted images," *Front. Neuroinform.,* vol. 8, pp. 1-11, 2014.

[14] A. Anderson and J. Gore, "Analysis and correction of motion artifacts in diffusion weighted imaging," *Magn Res Med,* vol. 32, pp. 379-87, 1994.

[15] R. Bammer, S. Holdsworth, M. Aksoy and S. Skare, "Phase errors in Diffusion-Weighted Imaging; In: Diffusion MRI: Theory, Methods, and Applications," D. Jones, Ed., Oxford University Press, 2011, pp. 218-249.

[16] T. Trouard, Y. Sabharwal, M. Altbach and A. Gmitro, "Analysis and Comparison of Motion Correction Techniques in Diffusion Weighted Imaging," *J Magn Reson Imaging,* vol. 6, pp. 925-935, 1996.

[17] M. Aksoy, C. Forman, M. Straka, S. Skare, S. Holdsworth, J. Hornegger and R. Bammer, "Real-time optical motion correction for diffusion tensor imaging," *Magn Res Med,* vol. 66, pp. 366-378, 2011.

[18] T. Benner, A. van der Kouwe and A. Sorensen, "Diffusion imaging with prospective motion correction and reacquisition," *Magn Reson Med,* vol. 66, pp. 154-167, 2011.

[19] M. Herbst, J. Maclaren, M. Weigel, J. Korvink, J. Hennig and M. Zaitsev, "Prospective motion correction with continuous gradient updates in diffusion weighted imaging," *Magn Res Med,* vol. 67, pp. 326-338, 2012.

[20] R. Haralick, K. Shanmugam and I. Dinstein, "Textural features for image classification," *IEEE Trans. Systems Man Cybernet.,* vol. 3, p. 610–621, 1973.

[21] N. Elsaid, S. Royes, M. Stone, R. Gullapalli, J. Prince and J. Zhuo, "Phase-based motion detection for diffusion magnetic resonance imaging," in *ISMRM*, Honolulu, Hawaii, USA, 2017.

[22] H. Goldstein, Classical Mechanics, 2nd edition ed., MA: Addison-Wesley, 1980.

[23] V. Wedeen, R. Weisskoff and B. Poncelet, "MRI signal void due to in-plane motion is all-or-none," *Magn Res Med,* vol. 32, pp. 116-120, 1994.

[24] D. Jones, M. Horsfield and A. Simmons, "Optimal Strategies for Measuring Diffusion in Anisotropic Systems by Magnetic Resonance Imaging," *Magn Reson Med,* vol. 42, pp. 515-525, 1999.

[25] M. Jenkinson and S. M. Smith, " A global optimisation method for robust affine registration of brain images.," *Medical Image Analysis,* vol. 5, no. 2, pp. 143-156, 2001.

[26] M. Jenkinson, P. R. Bannister, J. M. Brady and S. M. Smith, "Improved optimisation for the robust and accurate linear registration and motion correction of brain images.," *NeuroImage,* vol. 17, no. 2, pp. 825-841, 2002.

[27] S. Smith, "Fast robust automated brain extraction," *Human Brain Mapping,* vol. 17, no. 3, pp. 143-155, 2002.

[28] R. Wang, T. Benner, A. Sorensen and V. Wedeen, "Diffusion toolkit: a software package for diffusion imaging data processing and tractography," in *ISMRM*, Berlin, Germany, 2007.

[29] N. M. H. Elsaid, R. P. Gullapalli, M. Stone, S. Roys, J. L. Prince and J. Zhuo, "Phase-based motion detection for diffusion magnetic resonance imaging (dMRI) of the tongue," in *ISMRM Workshop on Motion Correction in MRI & MRS*, Cape Town, South Africa, 2017.

[30] J. Deux, M. Maatouk, A. Vignaud, A. Luciani, G. Lenczner, J. Mayer, P. Lim, J. Dubois-Randé, H. Kobeiter and A. Rahmouni, "Diffusion-weighted echo planar imaging in patients with recent myocardial infarction," *Eur Radiol,* vol. 21, pp. 46-53, 2011.

15

[31] H. Shinagawa, E. Murano, J. Zhuo, B. Landman, R. Gullapalli, J. Prince and M. Stone, "Tongue muscle fiber tracking during rest and tongue protrusion with oral appliances: a preliminary study with diffusion tensor imaging.," *Acoust Sci Technol,* vol. 29, pp. 291-294, 2008.

[32] C. Pierpaoli, L. Walker, M. Irfanoglu, A. Barnett, P. Basser, L. Chang, C. Koay, S. Pajevic, G. Rohde, J. Sarlls and M. Wu, "TORTOISE: an integrated software package for processing of diffusion MRI data," in *ISMRM 18th annual meeting*, Stockholm, Sweden, 2010.

[33] P. Brynolfsson, D. Nilsson, T. Torheim, T. Asklund, C. T. Karlsson, J. Trygg, T. Nyholm and A. Garpebring , "Haralick texture features from apparent diffusion coefficient (ADC) MRI images depend on imaging and pre-processing parameters.," *Nature Sci Rep.,* vol. 7, no. 1, p. 4041, 2017.

[34] T. Löfstedt, P. Brynolfsson, T. Asklund, T. Nyholm and A. Garpebring, "Gray-level invariant Haralick texture features," *PLoS One,* vol. 14, no. 2, p. e0212110, 2019.

16

TABLE 1- EXPERIMENT 1

RATIO OF THE DETECTED MOTION CORRUPTED GRADIENT SLICES RELATIVE TO THE TOTAL NUMBER OF SLICES OF THE FIVE DIFFERENT VOLUNTEERS (V1-V5)

Volunteer	V1	V2	V3	V4	V5
Ratio of detected motion corrupted slices using the PITA-MDD method	1.15 %	1.28 %	2.84 %	1.23 %	0.83 %
Ratio of detected outliers by *eddy*	2.36%	1.7%	2.83%	1.33%	1%
Ratio of slices detected by both PITA-MDD and *eddy*	1.03%	1.25%	2.33%	1.18%	0.58%

TABLE 2 –EXPERIMENT 2

RATIO OF THE DETECTED MOTION CORRUPTED GRADIENT SLICES RELATIVE TO THE TOTAL NUMBER SLICES OF VOLUNTEER V1 IN THREE DIFFERENT RESOLUTIONS

Resolution	3 mm x 3 mm	2.5 mm x 2.5 mm	2 mm x 2 mm
Ratio of detected motion corrupted gradient slices using the PITA-MDD method	6.25%	1.15 %	0.8%
Ratio of detected outliers by *eddy*	6.63%	2.36%	1.4%
Ratio of slices detected by both PITA-MDD and *eddy*	5.35 %	1.03%	0.64%

17

Noise level	No noise			Gaussian noise with SD=5			Gaussian noise with SD=15			Gaussian noise with SD=25			Gaussian noise with SD=35			Gaussian noise with SD=45			Gaussian noise with SD=55		
Resolution in isotopic mm	3	2.5	2	3	2.5	2	3	2.5	2	3	2.5	2	3	2.5	2	3	2.5	2	3	2.5	2
Ratio of detected motion corrupted slices using the PITA-MDD method	6.25%	1.15%	0.8%	6.25%	1.17%	0.81%	6.35%	1.25%	0.81%	6.39%	1.43%	0.84%	6.53%	1.71%	0.93%	6.77%	2.07%	1%	7.12%	2.57%	1.15%
Ratio of detected outliers by *eddy*	6.63%	2.36%	1.4%	6.63%	2.36%	1.52%	6.63%	2.28%	1.45%	6.63%	2.18%	1.45%	6.49%	1.95%	1.37%	6.15%	1.89%	1.3%	6.08%	1.85%	1.32%
Ratio of slices detected by both PITA-MDD and *eddy*	5.35%	1.03%	0.64%	5.31%	1.03%	0.66%	5.38%	1.04%	0.66%	5.07%	1.04%	0.66%	5.38%	1.02%	0.64%	5.28%	1.02%	0.66%	5.24%	1%	0.7%

18

TABLE 3 – NOISE SIMULATION

RATIO OF THE DETECTED MOTION CORRUPTED GRADIENT SLICES RELATIVE TO THE TOTAL NUMBER OF SLICES OF VOLUNTEER V1 IN THREE DIFFERENT RESOLUTIONS AND WITH ADDED GAUSSIAN RANDOM NOISE WITH ZERO MEAN AND SIX LEVELS OF STANDARD DEVIATIONS

20

FIGURE CAPTIONS

Fig. 1. An example of DW (a) magnitude images with some motion corrupted slices and (b) their corresponding phase counterparts; notice the phase images encompassed by red containers as they are corresponding to magnitude images with signal dropouts.

Fig. 2. A flow chart showing the main processing stages used in the PITA-MDD algorithm: T is the cut-off threshold.

Fig. 3. Three GLCM examples, (a) shows a magnitude DWI image with no motion, (b) shows the phase image corresponding to (a). (c) shows the computed GLCM of (b), it is mostly a diagonal matrix. (d) shows a magnitude DWI image with some subtle motion that cannot be detected using the magnitude images, (e) shows the phase image corresponding to (d). (f) shows the computed GLCM of (e). (g) shows a magnitude DWI image with severe motion, (h) shows the phase image corresponding to (g). (i) shows the computed GLCM of (h).

Fig. 4. (a) Homogeneity textural features extracted from the DW phase images of the five volunteers, with arrows pointing to the slices corrupted with motion, and when the subject pressed the button for motion notification. The x-axis represents the slice index, i.e., for 54 slices with a total of 67 volumes and 2 repetitions, the total number of acquired slices is 54 × 67 × 2 = 7236 slices. The right column shows the histograms of the homogeneity indices in the datasets of the five volunteers.

Fig. 4. (b) Homogeneity textural features extracted from the DW phase images of V1 3 mm x 3 mm, 2.5 mm x 2.5, and 2 mm x 2 mm slices, 2mm x 2 mm with no motion respectively. The right column shows the histograms of the homogeneity indices in the four cases.

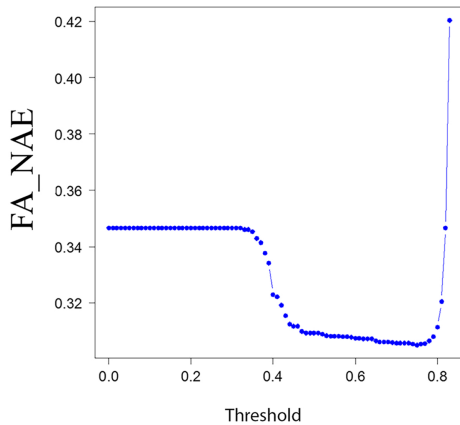Fig. 5. Validation results showing the NAE between the FA maps of the motion rejected data and that of the ground truth versus the threshold. (a) V1 (3 mm x 3 mm) results, (b) V1 (2.5 mm x 2.5 mm) results, (c) V1 (2 mm x 2 mm) results, (d) V2 results (e) V3 results, (f) the mean square error (MSE) of the results of a-e with the minimum threshold T.

Fig. 6. Colored FA of V1 through V5 with (a), and (b) showing a coronal slice and their corrected versions using the PITA-MDD method, respectively. Similarly, (c) and (d) show an axial slice and their corrected versions using the PITA-MDD method, respectively.

Fig. 7. (a) Tractography with a seed of 1.25 voxel radius placed in the Genu of the corpus callosum. The upper row shows datasets including slices corrupted with motion. The lower row shows datasets with motion-corrupted slices eliminated from diffusion mapping calculations. V1 through V5 are the datasets of the five volunteers. (b) Tractography with a seed of 1.25 voxel radius placed in the Genu of the corpus

21

callosum. The upper row shows datasets including slices corrupted with motion. The lower row shows datasets with motion-corrupted slices eliminated from diffusion mapping calculations. Columns I, II, and III are datasets corresponding to the V1 volunteer with 3 mm x 3 mm, 2.5 mm x 2.5, and 2 mm x 2 mm slices, respectively.

Fig. 8. A Comparison of the PITA-MDD elimination versus *eddy* elimination of some corrupted slices. In both (a) and (b), the first row shows the magnitude images of some of the DWI of V1 at 2mm x 2mm. The second row shows the corresponding phase images of the same slices. The third row compares the phase- and magnitude-based eliminations of the above slices, where the blue bar means the slice is rejected using the PITA-MDD method, and the orange bar means the slice is rejected using *eddy*. (a) is an example of a slice detected by PITA-MDD while not considered as an outlier by *eddy*.
(b) is an example of some gradient slices detected as an outlier by *eddy* and not by PITA-MDD.

Fig. 9. A comparison between the magnitude and phase images of a DWI (a) with no noise added (SNR=16.7), (b) with added Gaussian random noise with zero mean and SD=15 (DWI SNR=2.32), (c) with added Gaussian random noise with zero mean and SD=35 (DWI SNR=1.02), (d) with added Gaussian random noise with zero mean and SD=55 (DWI SNR=0.67).

Fig. 10. HHI of three slices range between 0.65 and 0.685 (a) and 0.92 and 0.98 (b), with added Gaussian random noise with zero mean and SD that varies between 0 and 60 in three different resolutions, 3mm x 3mm (acquird on Tim Trio scanner), 2.5mm x 2.5mm and 2mm x 2 mm (acquired on Prisma[fit] scanner). Also shown is the SNR of the corresponding DWI slice in the case of no added noise and in the case of added Gaussian random noise with SD of 60.
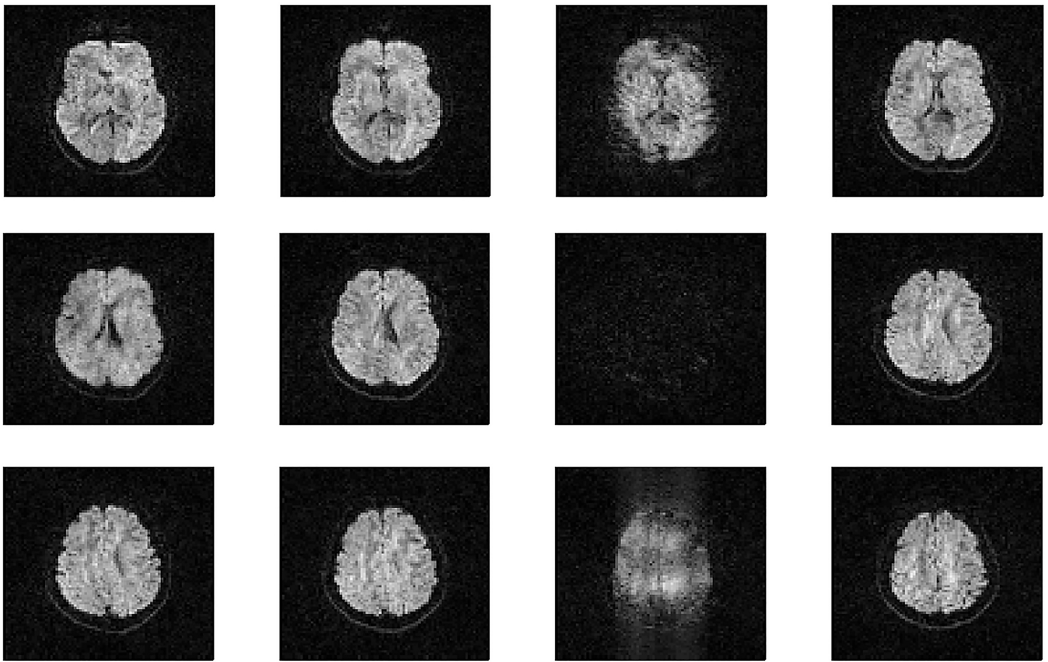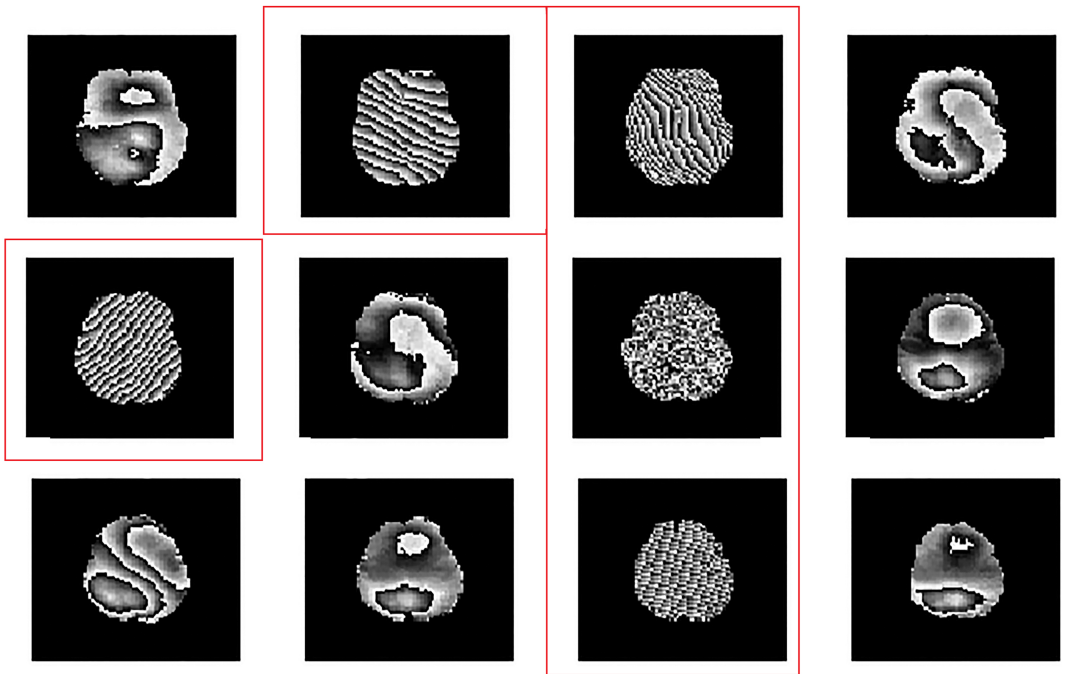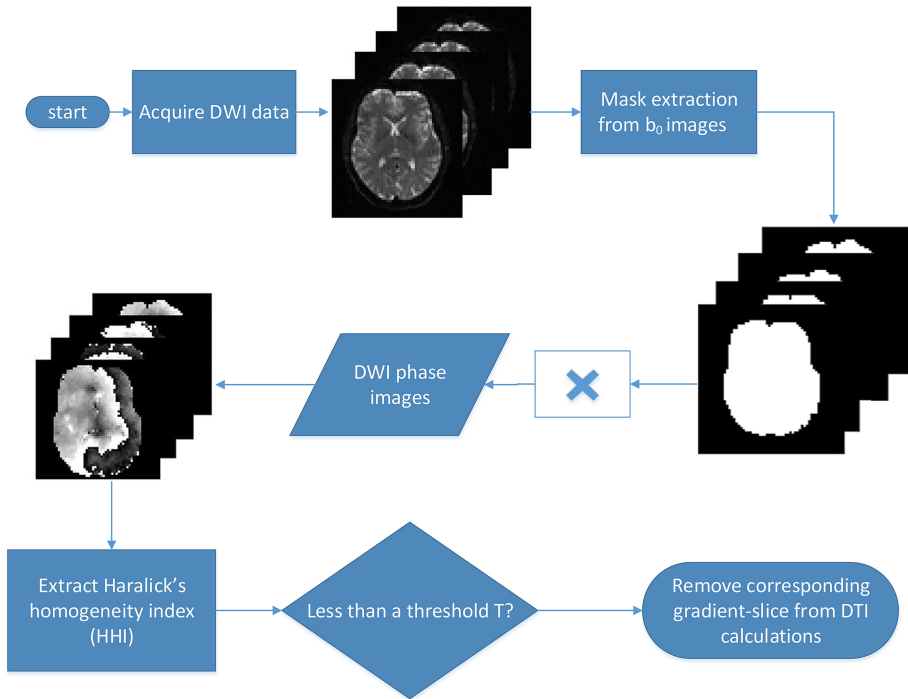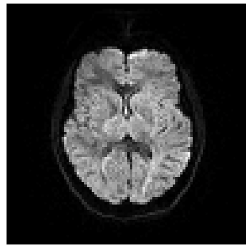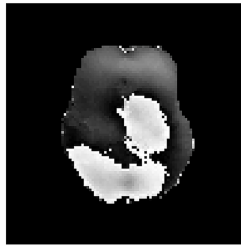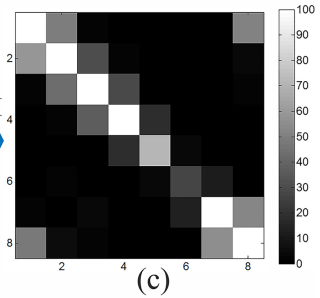
22

(a)

(b)

Figure 1

Figure 2

No motion

HHI=0.8628

GLCM

(a) (b) (c)

Subtle motion

HHI=0.4787

GLCM

(d) (e) (f)

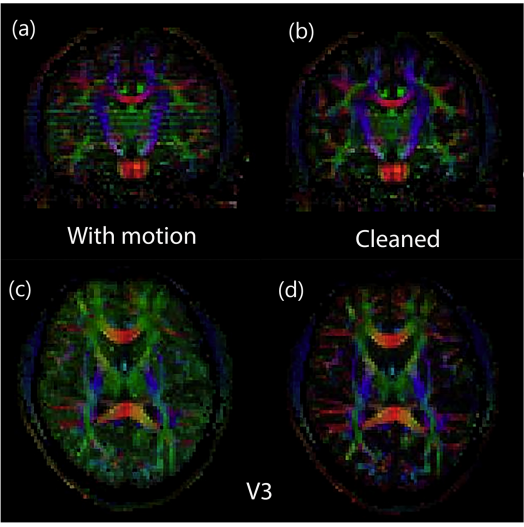Severe motion

HHI=0.37

GLCM

(g) (h) (i)

Figure 3

(a)

(b)

Figure 4

(a) V1 (3 mm x 3 mm)

(b) V1 (2.5 mm x 2.5 mm)

(c) V1 (2 mm x 2 mm)
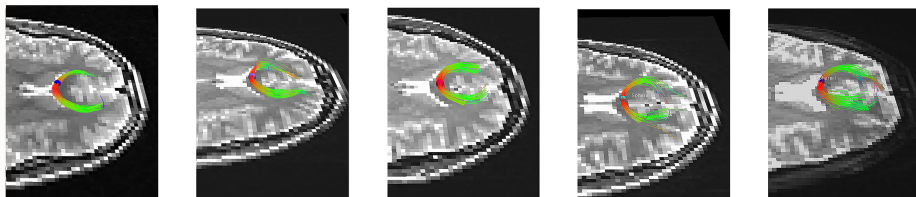
(d) V2

(e) V3
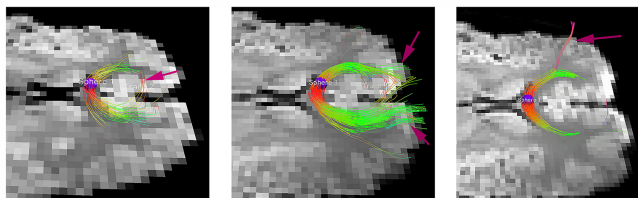
(f)

Figure 5

V1

V2

V3

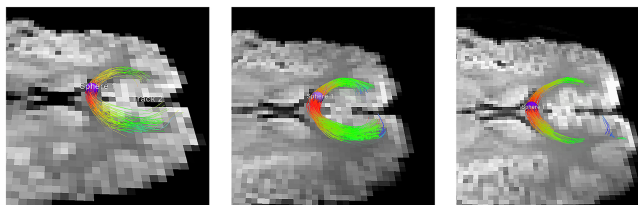V4

V5

Figure 6
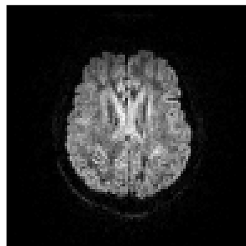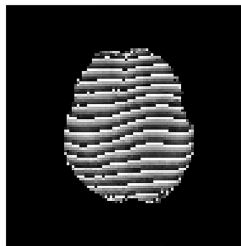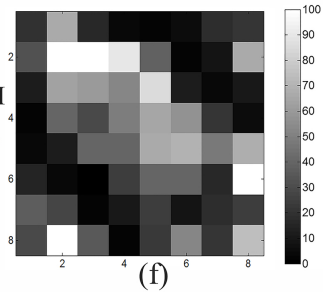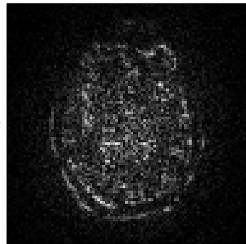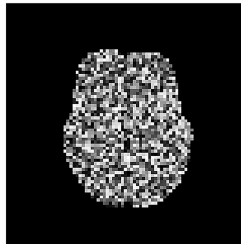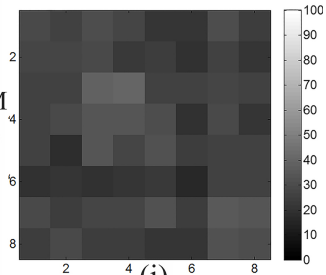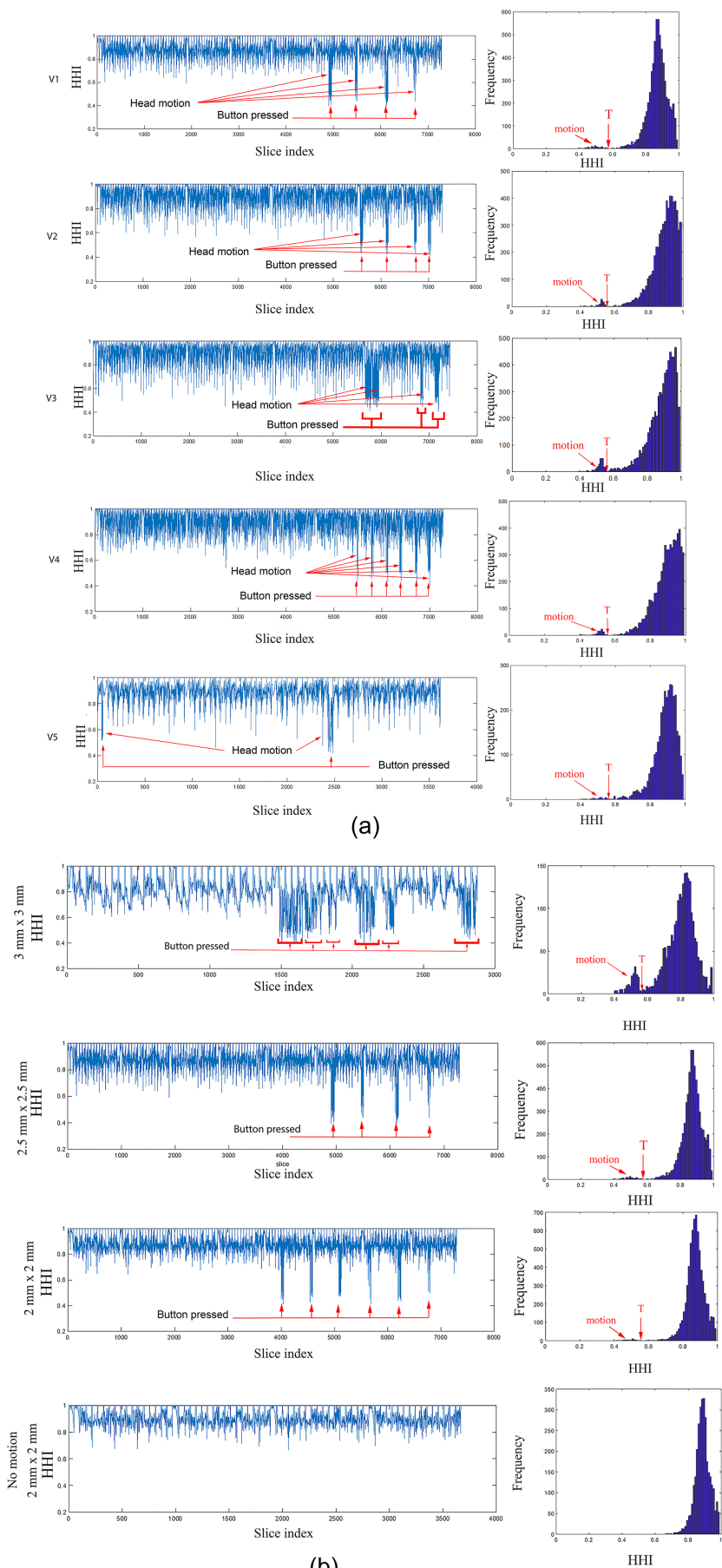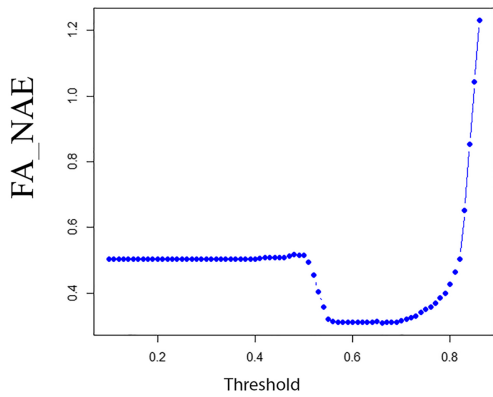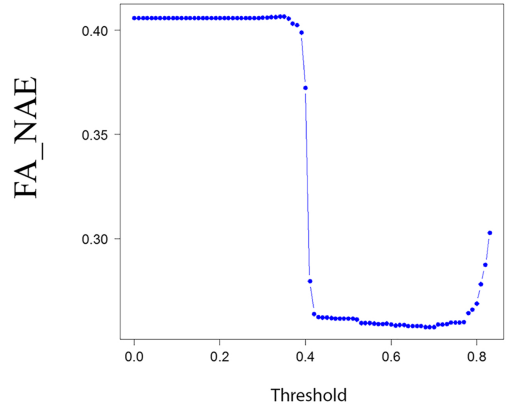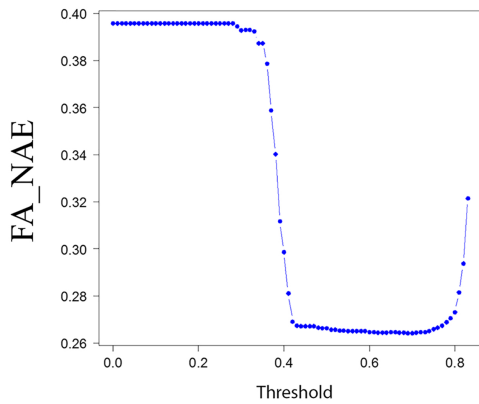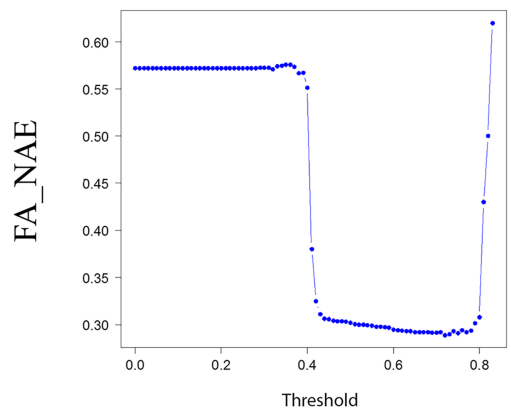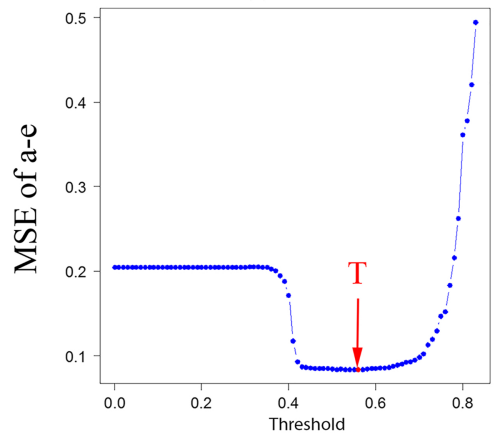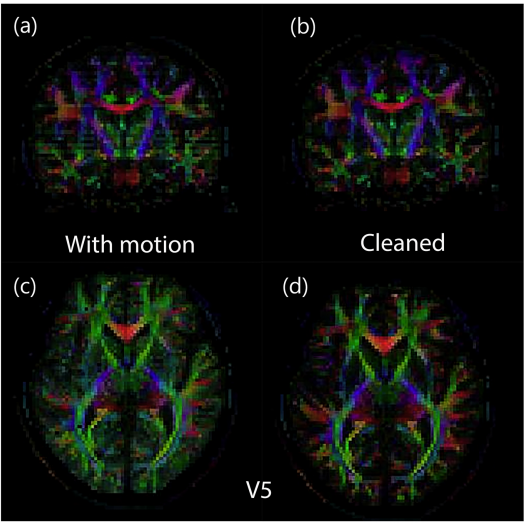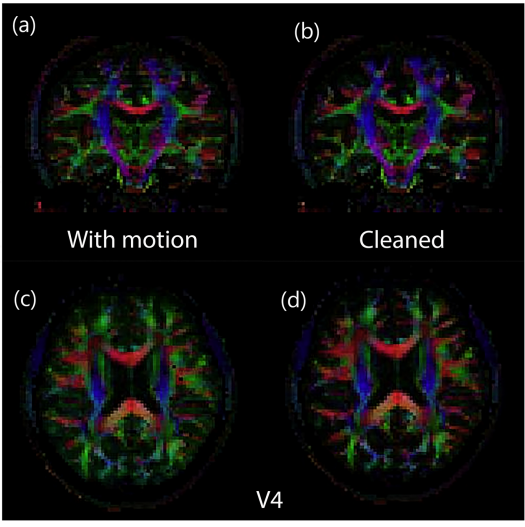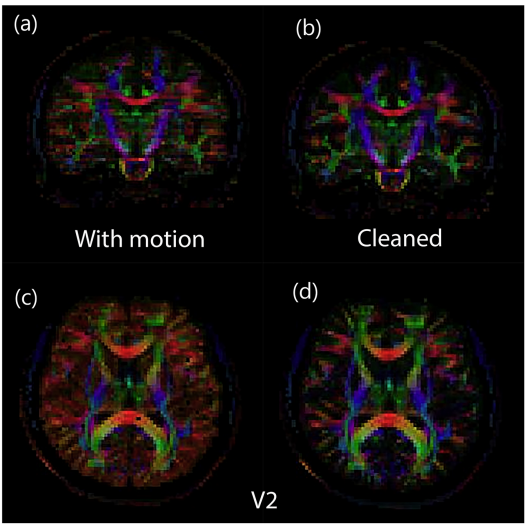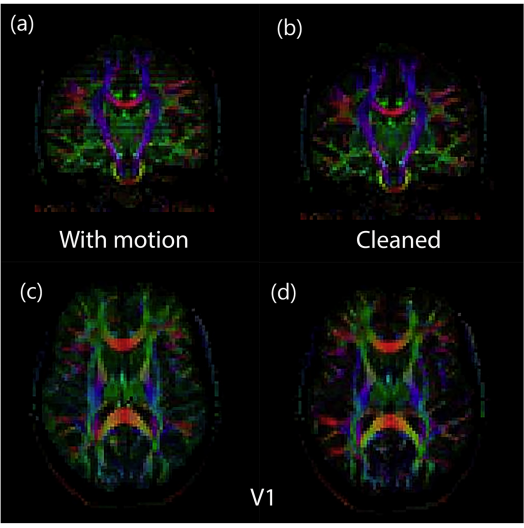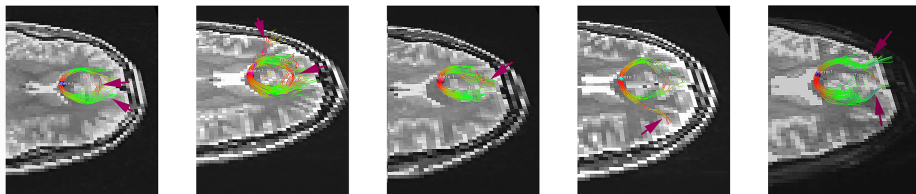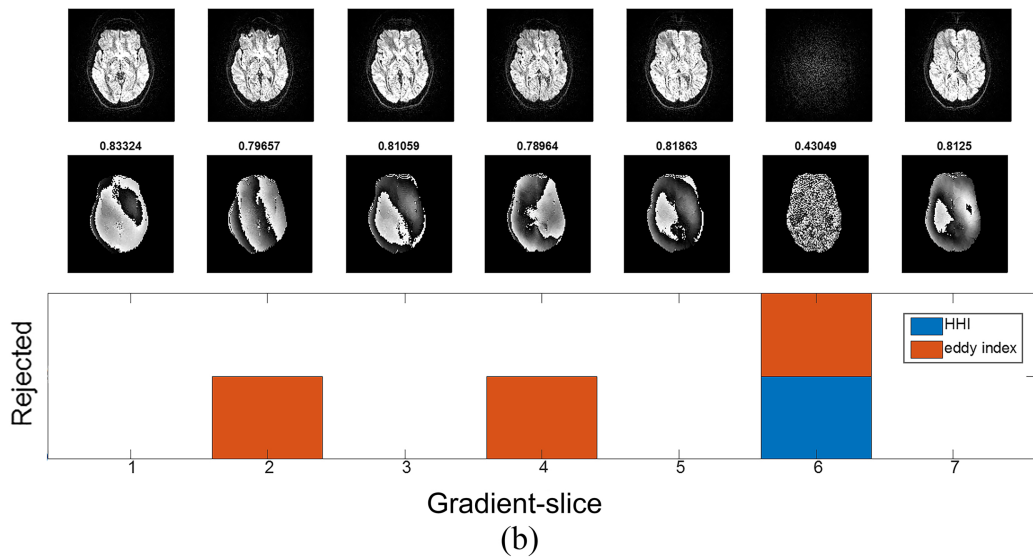
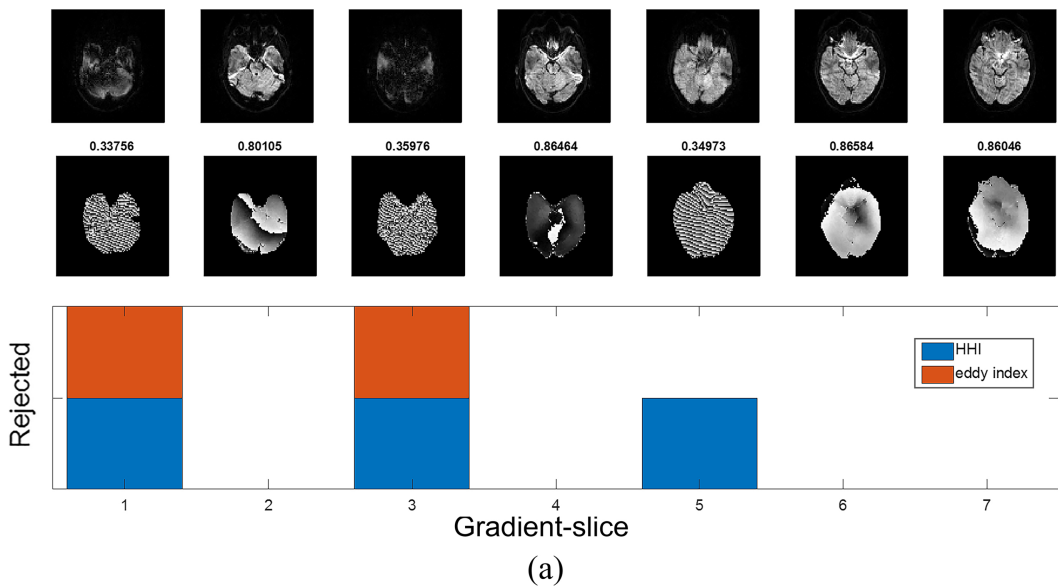With motion

Cleaned

V1   V2   V3   V4   V5

(a)

With motion

Cleaned
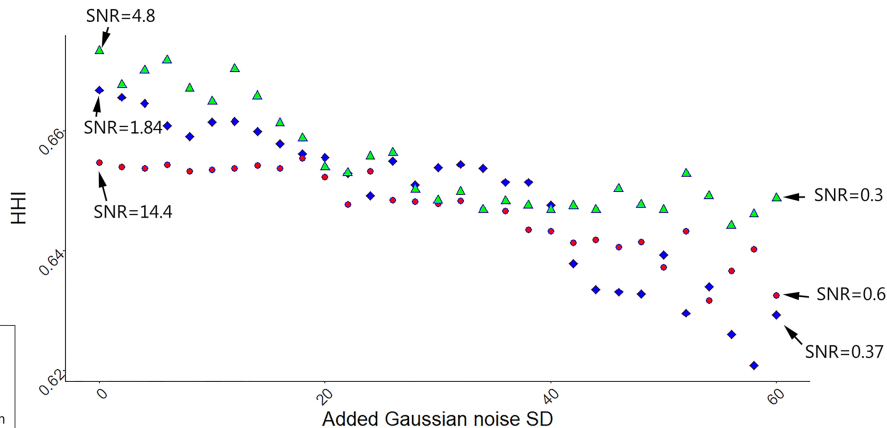
(I) 3 mm x 3 mm   (II) 2.5 mm x 2.5 mm   (III) 2 mm x 2 mm

(b)

Figure 7

(a)

(b)

Figure 8

Figure 9

(a)

(b)

Figure 10